**Title Page:**

---

**Submitted in:**
**Numerical Methods in Civil Engineering**

**Titel :**

# Numerical Investigation of Energy Dissipation and Hydraulic Performance of Slotted Roller Buckets with a Different Teeth Configuration

***Payam Heidarian*. Maryam Asadi**. Pouya Heidarian******

---

** Department of Civil, Environmental, Architectural Engineering and Mathematics, University of Brescia, 25123 Brescia, Italy.*
*** Department of Environmental Engineering, University of Tehran, Tehran, Iran.*
**** Department of Civil Engineering, University of Kharazmi, Alborz, Iran.*

**Statement:**
This paper is a non-peer reviewed preprint submitted to EarthArXiv. The manuscript has been submitted for peer review to the journal *Numerical Methods in Civil Engineering* and we are currently awaiting a decision on its acceptance.

Numerical Methods in Civil Engineering

# Numerical Investigation of Energy Dissipation and Hydraulic Performance of Slotted Roller Buckets with a Different Teeth Configuration

***Payam Heidarian*. Maryam Asadi**. Pouya Heidarian******

*ARTICLE INFO*

*Article history:*
*Received:*
---
*Revised:*
---
*Accepted:*
---

*Keywords:*
*Numerical Simulation*
*Energy Dissipator*
*Roller Bucket*
*FLOW-3D*
*CFD*

***Abstract:***

*The issue of scouring downstream of dams is one of the main topics that must be considered in the hydraulic design of structures. The enormous energy carried by the flow during spillway discharge, if not controlled, can cause severe erosion in the downstream area of the dam. To reduce the amount of scouring, it is necessary to examine the flow hydraulics and reduce turbulent energy and velocity in the flow direction while increasing the velocity in perpendicular directions to the flow, which leads to increased mixing. This can be achieved by using energy dissipators to reduce scouring. This study examines the roller bucket and the displacement of its teeth. In this manner, a roller bucket with zigzag teeth is used. The bucket and spillway were constructed using AutoCAD software and tested in FLOW-3D software to determine the modified hydraulics compared to aligned teeth. The results showed that the implemented changes decreased energy and velocity in the flow direction and increased the velocity perpendicular to the flow. It is evident that these results can reduce scouring in the downstream area of the bucket.*

.

## 1. Introduction

By constructing high dams along rivers, the discharge of surplus floodwater beyond the capacity of the dam reservoir is carried out through spillways. Given that spillways transform the flow from subcritical to supercritical state, the kinetic energy of the flow at the end of the spillway is significant and can cause erosion in the downstream riverbed of the spillway, endangering the stability of the dam and spillway. This concern can extend to the surrounding rivers [1]. Therefore, spillways require structures at the outlet end to dissipate energy, reducing the excess energy of the outlet flow, resulting in minimizing scour and erosion downstream of the spillway [2]. One of the solutions is using aeration at the end of the spillway to dissipate energy of water [3]. Another feasible solution is dissipating structure. One type of energy dissipating structure that has gained significant attention from designers is Roller deflectors. The excess energy of the flow at the bottom of the Roller deflector structure leads to scour in the sediment bed [4].

In this context, numerous studies have been conducted on scour caused by jet flows. Many studies have investigated the loss of energy in soil which could be considered in scouring energy loss [5~7]. Mason and Arumugam (1985) compiled and analyzed all the equations that researchers had presented for estimating the maximum depth of scour induced by jet flows, including equations by Veronese (1937), Chee and Padiyar (1969), Martins (1975) [8~11]. To determine the accuracy of the various equations, Mason and Arumugam (1985) utilized 47 sets of physical model data and 26 sets of field data, concluding that the equations by Martins (1975) the best results for the laboratory model data [8,11]. According to Mason and Arumugam (1985), incorporating the tailwater depth parameter enhances the accuracy of equations that only include parameters such as flow rate, drop height, and particle size, leading to the proposal of a new equation [8].

** Department of Civil, Environmental, Architectural Engineering and Mathematics, University of Brescia, 25123 Brescia, Italy.*
*** Department of Environmental Engineering, University of Tehran, Tehran, Iran.*
**** Department of Civil Engineering, University of Kharazmi, Alborz, Iran.*

Strelchuck (1969) investigated the scour downstream of a Roller bucket on a sandy bed. His experimental results indicated that doubling and tripling the flow rate increased the scour hole depth by 50% and 80%, respectively. Additionally, increasing the jet angle from 30 degrees to 45 degrees resulted in a 16% increase in maximum scour depth, attributed to the increased vertical velocity component caused by the steeper jet angle upon impacting the tailwater [12].

Azmathullah et al. (2005) predicted the maximum scour depth downstream of free-flow Roller buckets using artificial neural networks [13]. They found that the artificial neural network method provided more accurate predictions compared to conventional regression and empirical equations. Additionally, they emphasized the necessity of using information on the bucket's radius and angle, particle size, and tailwater depth, along with the required data for empirical equations, which include flow per unit width and drop height. The use of dimensionless variables yielded better results compared to raw variables.
It was observed that sediment diameter does not significantly impact the length and depth of scour, being primarily dependent on flow conditions [14]. However, generally, the minor effect of particle size is such that as the diameter increases, the length and depth of scour decrease. With an increase in tailwater depth, the influence of particle size quickly diminishes [14]. Golzari (2003) examined the impact of jet dispersion in toothed buckets and the effect of tailwater depth in controlling downstream scour of Roller energy dissipators of high dams. For this purpose, scour studies and optimization of the geometric design of Roller dissipators for the spillways of two dams in the country (Raeesali Delvari and Aq Chay) were conducted using physical models at the Water Research Center [15]. Amanian (1993) investigated the scour phenomenon downstream of Roller spillways through 64 experiments, selecting two types of particle diameters, a specific range of flow rates, three bucket edge angles, and five tailwater depths [16]. Additionally, in 2011, Panahi and et al. conducted laboratory studies on the impact of flow characteristics on downstream scour of simple submerged Roller buckets [17]. In 2011, Eshtiyaq Hasan Nejad and et al. conducted laboratory studies on downstream scour of toothed submerged Roller buckets [18]. Panahi and et al. (2012) compared scour in toothed and simple submerged Roller buckets [19].
In 2013, Gilson Peterson from Iceland conducted studies on the hydraulics of the flip bucket flow of the Urafoss hydropower plant using 2.5D and 3D laboratory and numerical models with ANSYS-CFX software, observing the effects of bucket level and tailwater depth [20]. In 1956, Malcolm Carr conducted experimental research on the hydraulics of a simple flip bucket, examining the impact of tailwater depth, chute slope, flow rate, and tailwater depth on the flow hydraulics passing through the bucket [21]. Despite numerous studies, including Heidarian's 2022 numerical study, the rules and analyses on this topic are still incomplete, and there is a notable lack of numerical studies in this area [22]. This research investigates the effects of different tooth arrangements using FLOW-3D software.

## 2. Methodes

In this study, the FLOW-3D software was utilized for simulating the flow field in a flip bucket, considering the capabilities, features, and limitations of available software. The governing equations for the movement of incompressible viscous fluid in a turbulent state are expressed by the Reynolds-averaged Navier-Stokes (RANS) equations. Given that the flow downstream of the spillway is always highly turbulent, the RANS equations with a two-equation turbulence model were employed to solve the turbulent flow and calculate turbulence transport within the computational domain [23]. It is worth noting that the second-order upwind method was used to solve the governing equations for advection and diffusion. In the Cartesian coordinate system, the governing equations are the continuity equation and the momentum equation, which are presented below [24&25].

(1)

$$V_F \frac{\partial \rho}{\partial t} + \frac{\partial}{\partial x}(\rho u A_x) + R\frac{\partial}{\partial y}(\rho v A_y) + \frac{\partial}{\partial z}(\rho w A_z) + \xi \frac{\rho u A_x}{X} = R_{DIF} + R_{SOR}$$

Where $V_F$ is the volumetric void fraction ratio of open space to flow, $\rho$ is the fluid density, $R_{DIF}$ represents turbulent diffusivity, and $R_{SOR}$ denotes the mass source term. $u$, $v$, and $w$ are velocity components,

while $A_x, A_y, A_z$ denote the cross-sectional areas in the *x*, *y*, and *z* directions respectively.
The momentum equations are as follows:

$$\frac{\partial U_i}{\partial t} + \frac{1}{V_F}\left(U_i A_i \frac{\partial U_i}{\partial x_i}\right) = \frac{1}{\rho}\frac{\partial \acute{P}}{x_i} + g_i + f_i \quad (2)$$

In the above equations, $\acute{P}$ represents pressure, $g_i$ denotes the gravitational force in the direction i, and $f_i$ represents the Reynolds stress.

### *1.1 Modeling Free Surface Flow*

In this study, the Volume of Fluid VOF model has been utilized to determine the free surface. The VOF model can track the free surface and impose appropriate boundary conditions on those surfaces. For air-water flow, the parameter F represents the volume fraction of water, and its complement 1 – F denotes the volume fraction of air. The fluid volume equations within a unit volume are expressed as [26&27]:

$$\frac{\partial F}{\partial t} + \frac{1}{V_F}\left[\frac{\partial}{\partial x}(FA_x u) + \frac{\partial}{\partial y}\left(FA_y v\right) + \frac{\partial}{\partial z}(FA_z w)\right] = F_{DIF} + F_{SOR} \quad (3)$$

where $F_{SOR}$represents the temporal rate of change of the volume fraction of water associated with the mass source $R_{SOR}$, and the diffusion term is given by [12]:

$$F_{DIF} = \frac{1}{V_F}\left[\frac{\partial}{\partial x}\left(\vartheta_f A_x \frac{\partial F}{\partial x}\right) + \frac{\partial}{\partial y}\left(\vartheta_f A_y \frac{\partial F}{\partial y}\right) + \frac{\partial}{\partial z}\left(\vartheta_f A_z \frac{\partial F}{\partial z}\right)\right] \quad (4)$$

And the diffusion coefficient is $\vartheta_f = \frac{c_f \mu}{\rho}$, where $c_f$ is a constant dependent on the Schmidt number [26].

### *1.2. RNG Turbulence Model*

The RNG turbulence model is based on a precise statistical technique and mathematical relationships. In this model, compared to the standard approach, an additional term is introduced into the equation, which enhances the computational accuracy in turbulent flows [28 & 29]. Unlike the standard model, RNG demonstrates higher efficiency in rotational flows, and analytical relations are used to determine the turbulence parameters. Therefore, this model provides suitable accuracy at low Reynolds numbers and is commonly used to determine turbulence quantities in fields with geometric complexity or curvature. The governing equations in this model are formulated as follows [30]:
Equation for k:

$$\rho\frac{Dk}{Dt} = \frac{\partial}{\partial x_i}\left[\alpha_k \mu_{eff}\frac{\partial k}{\partial x_i}\right] + G_k + G_b - \rho\varepsilon \quad (5)$$

Equation for ε:

$$\rho\frac{D\varepsilon}{Dt} = \frac{\partial}{\partial x_i}\left[\alpha_\varepsilon \mu_{eff} + \frac{\partial \varepsilon}{\partial x_i}\right] + C_{1\varepsilon}\frac{\varepsilon}{k}\left(G_k + G_{3\varepsilon}G_b\right) - C_{2\varepsilon}\rho\frac{\varepsilon^2}{k} - R \quad (6)$$

The effective eddy viscosity $\mu_{eff}$ in the above equations is determined by the following relationships:

$$\bar{v} = \frac{\mu_{eff}}{\mu} \; and \; d\left(\frac{\rho^2 k}{\sqrt{\varepsilon\mu}}\right) = 1.72\frac{\bar{v}}{\sqrt{\left(\bar{v} - (1 + c_v)\right)}}d\bar{v} \quad (7)$$

In this equation, k is the turbulent kinetic energy, ρ is the fluid density, and ε is the turbulence dissipation rate .
If the above differential equation is integrated, the eddy viscosity can be determined, which, at high Reynolds numbers, simplifies to the relationship:

$$\mu_t = pC_u\frac{k^2}{\varepsilon}$$

However, at low Reynolds numbers, particularly near the wall, the differential form can be used directly. The inverse turbulent Prandtl number $a_\varepsilon$, $a_k$ is determined based on the following relationship:

$$\left|\frac{\alpha - 1.3929}{\alpha_0 - 1.3929}\right|^{06321} \times \left|\frac{\alpha + 2.3929}{\alpha_0 + 2.3929}\right|^{0.3679} = \frac{\mu_{mol}}{\mu_{eff}} \quad (8)$$

In high Reynolds number flows where the flow is fully turbulent, $\frac{\mu_{mol}}{\mu_{eff}} \ll 1$ holds, $a_0 = 1$ and the inverse turbulent Prandtl numbers remain constant, i.e,.

$$a_\varepsilon = a_k \approx 1.393$$

The additional term R included in the RNG model, compared to the standard model, refines the equation in regions with high strain rates and is defined by the following relationship:

$$R = \frac{C_\mu \rho \eta^3 \left(1 - \eta/\eta_0\right)}{1 + \beta \eta^3} \frac{\varepsilon^2}{K} \qquad (9)$$

In the above equations, $\eta = SK/\varepsilon$, and $S$ represents the modulus of the mean strain rate, which is defined in terms of the mean strain rate as follows:

$$S \equiv \sqrt{2S_{ij}^2} \quad , \quad S_{ij} = \frac{1}{2}\left(\frac{\partial u_i}{\partial x_j} + \frac{\partial u_j}{\partial x_i}\right) \qquad (10)$$

where $S_{ij}$ is the mean strain rate tensor.
The constants for the equations are as shown in the following table (Table1):

**Table 1:** Constants for the RNG state of the $k - \varepsilon$ model

| $C_\mu$ | $C_{1\varepsilon}$ | $C_{2\varepsilon}$ | $C_v$ | $\eta_0$ | $\beta$ |
|---|---|---|---|---|---|
| 0/0854 | 1/42 | 1/68 | 100 | 4/38 | 0/012 |

## 3. Numerical Solution

The present research numerically investigates the effect of tooth displacement on the hydraulics of flow passing through a slotted roller bucket using FLOW-3D software. Initially, it was necessary to calibrate and validate the software, which was done using the laboratory model of Ferguson and Carr (1956). In their study on a roller bucket with two chute designs, two buckets, and a channel, they examined the effect of variations in discharge, tailwater depth, chute slope, and bucket radius on the flow hydraulics [21].

Two experiments from this study were selected, and the geometry of the chute and bucket was created in AutoCAD software. Flow conditions such as discharge, boundary conditions, tailwater depth, and initial head were entered into FLOW-3D software according to the experimental conditions of the aforementioned study, and the model was run using FLOW-3D. One experiment was used for calibration, and another for validation. After ensuring the correct functioning of the software, the effect of the tooth arrangement parameter on the flow hydraulics and energy was investigated [31 & 32].

The aim of this work was to identify the creation of greater interference in the flow pattern and reduce the velocity and turbulence in the flow. In these models, the bucket with 45-degree launch angle teeth was constructed in two types. One was with teeth in the standard design according to the roller bucket of the Urriðafoss Hydropower Plant dam, and the other was the same bucket with the difference that the teeth were shifted back and forth in a zigzag pattern.

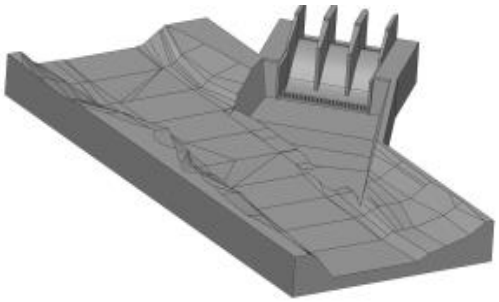

**Fig. 1:** 3D model of the spillway, channel, and downstream riverbed of the Urriðafos Hydropower Plant

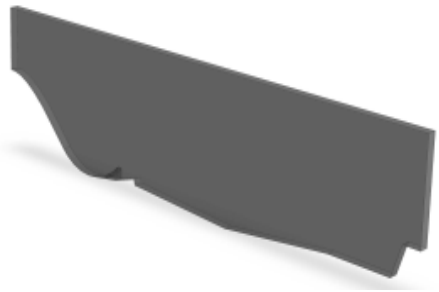

**Fig. 2:** 2.5D model of the spillway and bucket of the Urriðafos Hydropower Plant

An unstructured block meshing approach was used to discretize the solution domain, comprising approximately six hundred thousand computational volumes. Finer meshes were utilized in regions with significant flow parameter variations, while coarser meshes were applied in other areas. Figure 3 illustrates the solid boundaries and meshing of the numerical spillway model.

For the inlet boundary, discharge and specified input depth conditions were chosen, which are consistent across all models and match the validation source. The outlet boundary condition was set to constant pressure.

It is important to note that constant pressure in FLOW-3D can influence flow conditions. However, if the boundary is placed far from the region of interest, it will not affect the study located at a distance [33, 34, 35]. In this model, the channel length was extended sufficiently so that the constant pressure boundary condition does not impact the flow hydraulics at the section of interest. The side boundary condition was set as a wall.

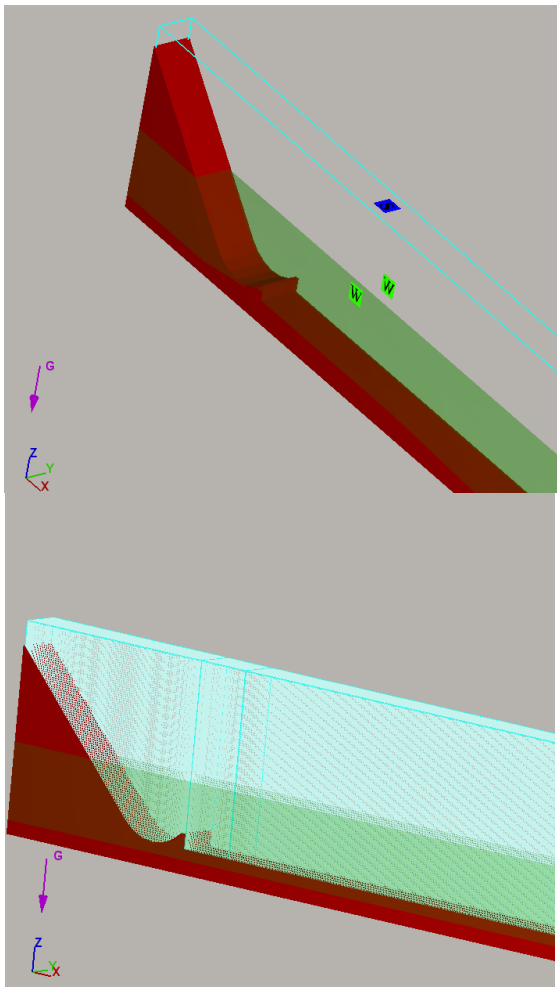

**Fig. 3:** Solid boundaries, geometry, and meshing of the solution domain for validation models

For the separation of the solution field, a non-uniform block meshing strategy was employed, totaling approximately six hundred thousand computational volumes. In regions with significant variations in flow parameters, finer meshes were used, while coarser meshes were applied elsewhere. Figure 3 illustrates the solid boundaries and meshing of the numerical spillway model.

For the inlet boundary, conditions were set for flow rate and depth based on the validation experiments, consistent across all models. A fixed pressure condition was specified for the outlet boundary. It's worth noting that a fixed pressure boundary in FLOW 3D can influence flow conditions. However, placing the boundary far from the study area ensures minimal effect on the study conducted at a distance [2 & 28].

In this model, the length of the channel was considered sufficient to ensure that the fixed pressure boundary condition had negligible impact on the hydraulic flow at the desired cross-section. The side boundaries were set as solid walls.

Tables 2 and 3 demonstrate the agreement between the results of the models developed in FLOW 3D and those from the experimental studies by Ferguson and Carr (1956) [19]. Based on Firozjaei et al. [36] and Aghazadeh et al. [37&38], the error values are in the acceptable range. As a result, the numerical model can be considered reliable

For validation and calibration, two laboratory models were used. It is important to note that in this entire research, the x-axis represents the flow direction, the z-axis represents the height and depth of the flow, and the y-axis represents the transverse direction to the flow.

Using an experiment conducted by Carr (1956) [21] with a tailwater depth of 3 feet, the numerical model was calibrated. The validation of the numerical model was performed using another experiment from their studies with a tailwater depth of 2 feet. In their experiments, they only provided the depth at three points, which were used for calibration and validation.

In the main models where the toothed bucket is examined, the boundary conditions were chosen similar to the 2.5D model created from the roller bucket of the Urriðafoss Hydropower Plant in Iceland. A symmetry boundary condition was subsequently applied to allow the model, with a narrow width, to be generalized to greater widths.

**Table 2:** Comparison of the results of the calibrated numerical model with the experimental model

| $h_2$ | $h_b$ | $h_s$ | $h_b/h_1$ | $h_2/h_1$ | $h_s/h_1$ | $h_b/h_2$ | $q/\sqrt{g}h_2^{1.5}$ | |
|---|---|---|---|---|---|---|---|---|
| 3 | 2/95 | 3/35 | 0/399 | 0/405 | 0/452 | 0/98 | 0/043 | Experimental |
| 2/98 | 2/77 | 3/14 | 0/374 | 0/403 | 0/424 | 0/929 | 0/0436 | Numerical |
| 0/667 | 6/102 | 6/268 | 6/266 | 0/494 | 6/195 | 5/204 | 1/395 | Percentage Error |

**Table 3:** Comparison of the results of the numerical model with the experimental model for validation

| $h_2$ | $h_b$ | $h_s$ | $h_b/h_1$ | $h_2/h_1$ | $h_s/h_1$ | $h_b/h_2$ | $q/\sqrt{g}h_2^{1.5}$ | |
|---|---|---|---|---|---|---|---|---|
| 2/1 | 1/75 | 2/6 | 0/237 | 0/284 | 0/351 | 0/83 | 0/074 | Experimental |
| 2/099 | 1/735 | 2/25 | 0/234 | 0/284 | 0/304 | 0/826 | 0/0739 | Numerical |
| 0/048 | 0/857 | 13/461 | 1/072 | 0/124 | 13/375 | 0/411 | 0/133 | Percentage Error |

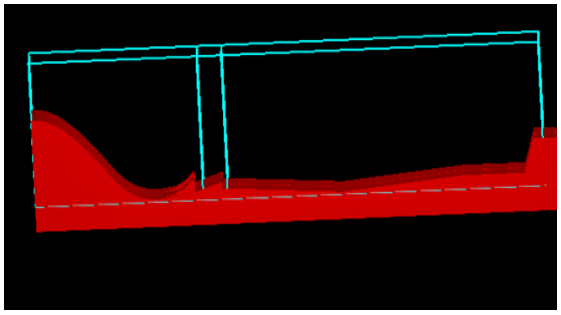

**Fig 4:** The model constructed based on the bucket and spillway of the Florence Hydropower Plant in Iceland

In Figure 4, the spillway model constructed with identical teeth in a single row was built based on the 2.5D model of the Florence Hydropower Plant bucket. This model was tested in Flow 3D software with one more tooth than the bucket model constructed by Petursson, which was designed in AutoCAD.

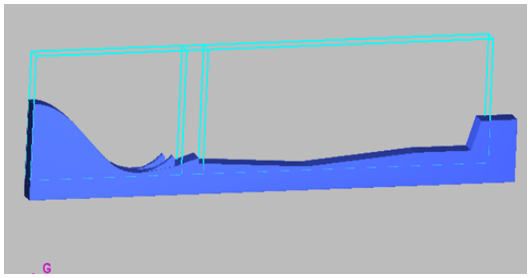

**Fig 5:** The bucket model with identical teeth, but shifted by a specific amount

In Figure 5, the constructed model with teeth arranged in a zigzag pattern and shifted by a specific amount is also shown.

## 4. Results and Discussion

It is worth mentioning that each run on a computer with a 3.5 GHz CPU and 12 GB of RAM took approximately 17 hours. As stated, throughout this research, the x-axis represents the flow direction, the z-axis represents the height and depth of the flow, and the y-axis represents the transverse direction to the flow.

After achieving flow stability (complete solution) and examining the streamlines, it was observed that in the case of identical teeth, the flow moves almost straight and without deviation from the x-axis. However, if the teeth are arranged in a zigzag pattern in a bucket, it can be seen that the flow becomes mixed and deviates to some extent from the x-axis. This mixing causes some of the energy that was used to accelerate the flow in the z and x directions to convert into velocity in the y direction. Consequently, while the velocities in the x and z directions decrease, the flow mixing increases, leading to greater energy dissipation. Obviously, with the reduction of energy, scouring also decreases. By reducing the flow velocity in the z direction, which is the component of velocity that lifts the sediment, this reduction can be interpreted as a decrease in scouring.

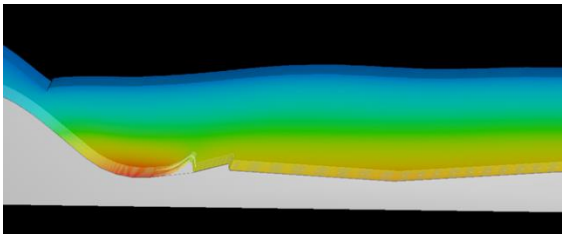

**Fig. 6:** The model implemented in FLOW-3D, a roller bucket with 45-degree teeth, designed based on the Urriðafoss Hydropower Plant dam.

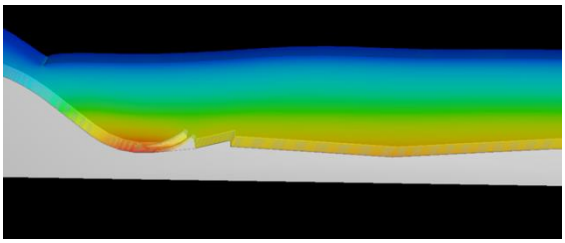

**Fig. 7:** The implemented model of a bucket with 45-degree teeth arranged in a zigzag pattern

In this model, the riverbed is positioned at an elevation of 6.5 centimeters, and if sediment is present, the minimum sediment height must be entered as 6.5 centimeters or higher. The velocities u, v, and z at elevations of 7.5, 10, 15, and 19.5 centimeters (shown as graphs between and on the teeth) are displayed. These velocities were examined on the teeth, in front of the bucket, at the deepest point of the bed, and

slightly ahead of it. In addition to the velocities, the dimensions of the vortices and the turbulence energy were also analyzed.

### *4.1 Streamwise Velocity (u):*

Figures (8 and 9) compare the streamwise velocity in both buckets.

- Elevation of 7.6 meters: According to the streamwise velocity (u) graphs, at an elevation of 7.6 meters (from the lowest point of the model), which is a location where sediment is likely present (if sediment is defined in the model), the velocity on the teeth (X=24.7) and slightly in front of the bucket (X=32.94) in the model with identical teeth (u1) is higher between the teeth and on both teeth compared to the bucket with staggered teeth (u2). Further along the channel at this depth, the velocity is nearly the same in both buckets.
- Elevation of 10.2 meters: At this elevation from the lowest point of the model, which is slightly above the teeth, the velocity in the bucket with identical teeth (u1) is higher at most points along the channel and bucket compared to the bucket with staggered teeth.
- Elevation of 15 meters: At this elevation, where it can be asserted that there will be no sediment at this depth, the velocity on the bucket and teeth in the bucket with identical teeth (u1) is lower than in the bucket with staggered teeth. However, in front of the bucket and on the bed, the streamwise velocity is lower in the bucket with staggered teeth.
- Elevation of 19.5 meters: At this elevation, it was observed that the velocity variations in the bucket with staggered teeth are nearly the same as in the bucket with identical teeth at three transverse points (the retracted tooth, the forward tooth, and between them in the bucket with staggered teeth and their corresponding points in the bucket with identical teeth). The velocity (u2) is higher on the bucket and teeth and lower (u1) further along.

Regarding streamwise velocity, it can generally be stated that near the bed, the velocity is lower in the bucket with staggered teeth. This velocity is one of the components that contribute to scouring, and the change in tooth arrangement has significantly reduced this component, potentially contributing to a reduction in scouring.

### *4.3 Vertical Velocity (w):*

According to the vertical velocity graphs in Figures (12 and 13), it can be generally stated that near the bucket and teeth, this velocity is significantly lower in the bucket with staggered teeth at lower depths (7.6 and 10.2 meters) and slightly higher on the bed compared to the bucket with aligned teeth. This indicates that the turbulence and boiling over the teeth and slightly ahead of them, which are the results of the vertical velocity component, have decreased with the change in tooth arrangement, leading to greater energy dissipation in this condition. Further ahead of the bucket (on the bed), the vertical velocity component is almost the same, with a slight reduction compared to the bucket with aligned teeth, indicating a decrease in the lifting power of the sediment-lifting component.
At greater depths (15 and 19.5 meters), this component changes slightly, with the bucket with staggered teeth having lower vertical velocities compared to the bucket with aligned teeth. Ultimately, by examining the velocities, it can be concluded that with the change in tooth arrangement, the streamwise velocity decreases, the transverse velocity perpendicular to the flow increases, and the vertical velocity also decreases.

### *4.2 Transverse Velocity (v):*

Figures (10 and 11) illustrate the effect of transverse velocity at different elevations.

- Elevation of 7.6 meters: At this elevation, the transverse velocity (v) on the bucket at the point on the forward tooth (in the bucket with staggered teeth) is nearly zero throughout the model. In contrast, in the bucket with aligned teeth, the transverse velocity on the teeth is significantly higher, and at other points on the bed throughout the model, it nearly matches the bucket with staggered teeth. Between the teeth and on the retracted tooth and its corresponding point in the aligned bucket, the transverse velocity is higher in the bucket with staggered teeth.

- Elevation of 10.2 meters: Clearly, at all points on the bed along the length and width at this elevation, the transverse velocity in the bucket with staggered teeth (v2) is higher than in the bucket with aligned teeth (v1). However, the velocities on the bucket and teeth are the same.
- Elevation of 15 meters: At this elevation, the conditions are similar to those at 10.2 meters, with the difference that the velocity differences between the buckets have increased.
- Elevation of 19.5 meters: The difference in transverse velocity between the buckets increases with distance from the bucket at this elevation. On the bucket and teeth, the transverse velocities at this level are nearly zero in both buckets. However, as the distance from the bucket increases, it is evident that the bucket with staggered teeth generates a higher transverse velocity at this elevation.

### *4.4 Turbulence Kinetic Energy (tke):*

Figure (14) shows the graphs of turbulence kinetic energy variations, which indicate turbulence. These graphs show the turbulence kinetic energy at all four elevations (7.6, 10.2, 15, and 19.5 meters) between the teeth. At all these elevations, the turbulence kinetic energy in the bucket with staggered teeth (tke2) is lower than in the bucket with aligned teeth (tke1). It can be asserted that with the increase in transverse velocity, the flow mixing has increased, and more energy has been dissipated. This leads to reduced flow turbulence downstream, resulting in a less turbulent flow.

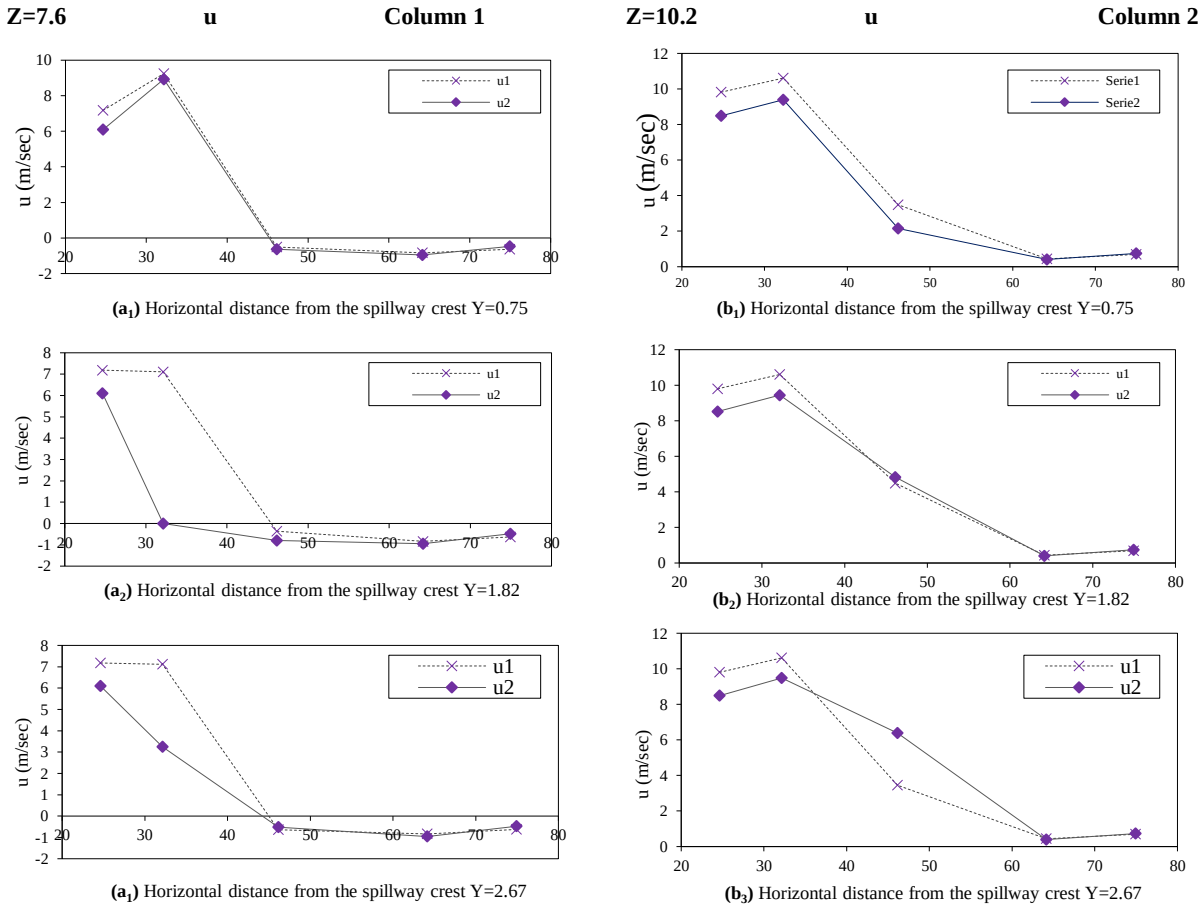


**Fig. 8:** The streamwise velocity at various points across the width of the bucket at **($a_{1, 2, \&3}$)** Z=7.6 and **($b_{1, 2, \&3}$)** Z=10.2 meters from the lowest point of the model. The measurements are taken at **($a_1$)** & **($b_1$)** Y=0.75 m (on the retracted tooth and its corresponding position in the bucket with aligned teeth), **($a_2$)** & **($b_2$)** Y=1.82 m (between the teeth), and **($a_3$)** & **($b_3$)** Y=2.67 m (on the forward tooth in the bucket with zigzag teeth and its corresponding position in the bucket with aligned teeth)

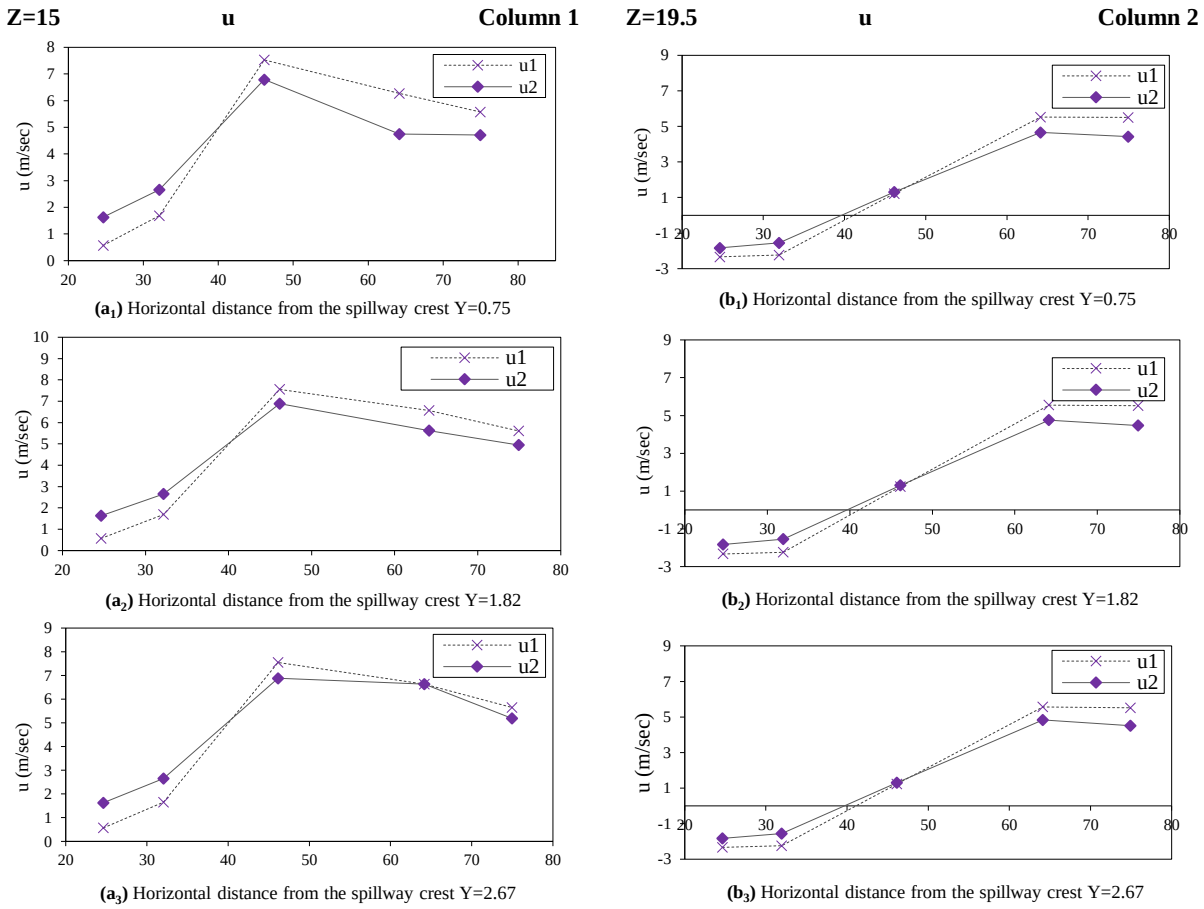


**Fig. 9:** The streamwise velocity at various points across the width of the bucket at **($a_{1, 2, \&3}$)** Z=15 and **($b_{1, 2, \&3}$)** Z=19.5 meters from the lowest point of the model. The measurements are taken at **($a_1$)** & **($b_1$)** Y=0.75 m (on the retracted tooth and its corresponding position in the bucket with aligned teeth), **($a_2$)** & **($b_2$)** Y=1.82 m (between the teeth), and **($a_3$)** & **($b_3$)** Y=2.67 m (on the forward tooth in the bucket with zigzag teeth and its corresponding position in the bucket with aligned teeth)

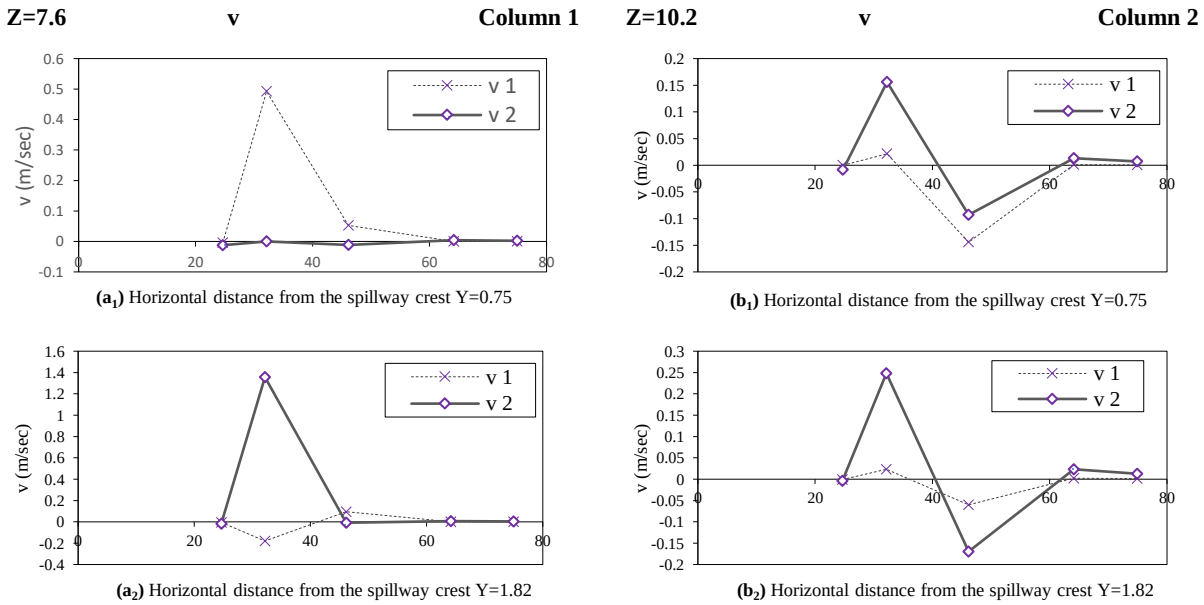

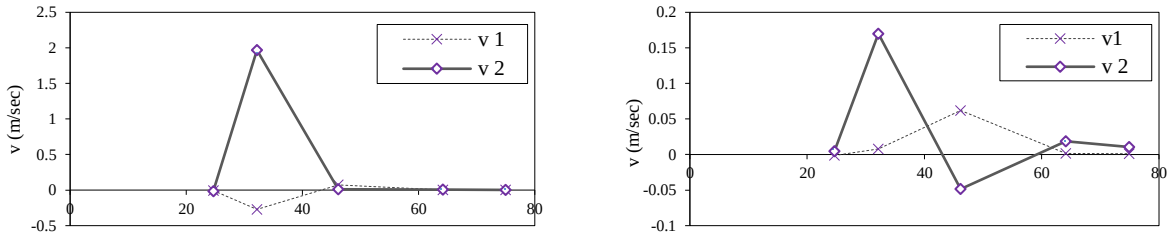


**($a_3$)** Horizontal distance from the spillway crest Y=2.67 **($b_3$)** Horizontal distance from the spillway crest Y=2.67

**Fig. 10:** The transverse velocity at various points across the width of the bucket at **($a_{1, 2, \&3}$)** Z=7.6 and **($b_{1, 2, \&3}$)** Z=10.2 meters from the lowest point of the model. The measurements are taken at **($a_1$)** & **($b_1$)** Y=0.75 m (on the retracted tooth and its corresponding position in the bucket with aligned teeth), **($a_2$)** & **($b_2$)** Y=1.82 m (between the teeth), and **($a_3$)** & **($b_3$)** Y=2.67 m (on the forward tooth in the bucket with zigzag teeth and its corresponding position in the bucket with aligned teeth)

**Z=15 v Column 1** **Z=19.5 v Column 2**

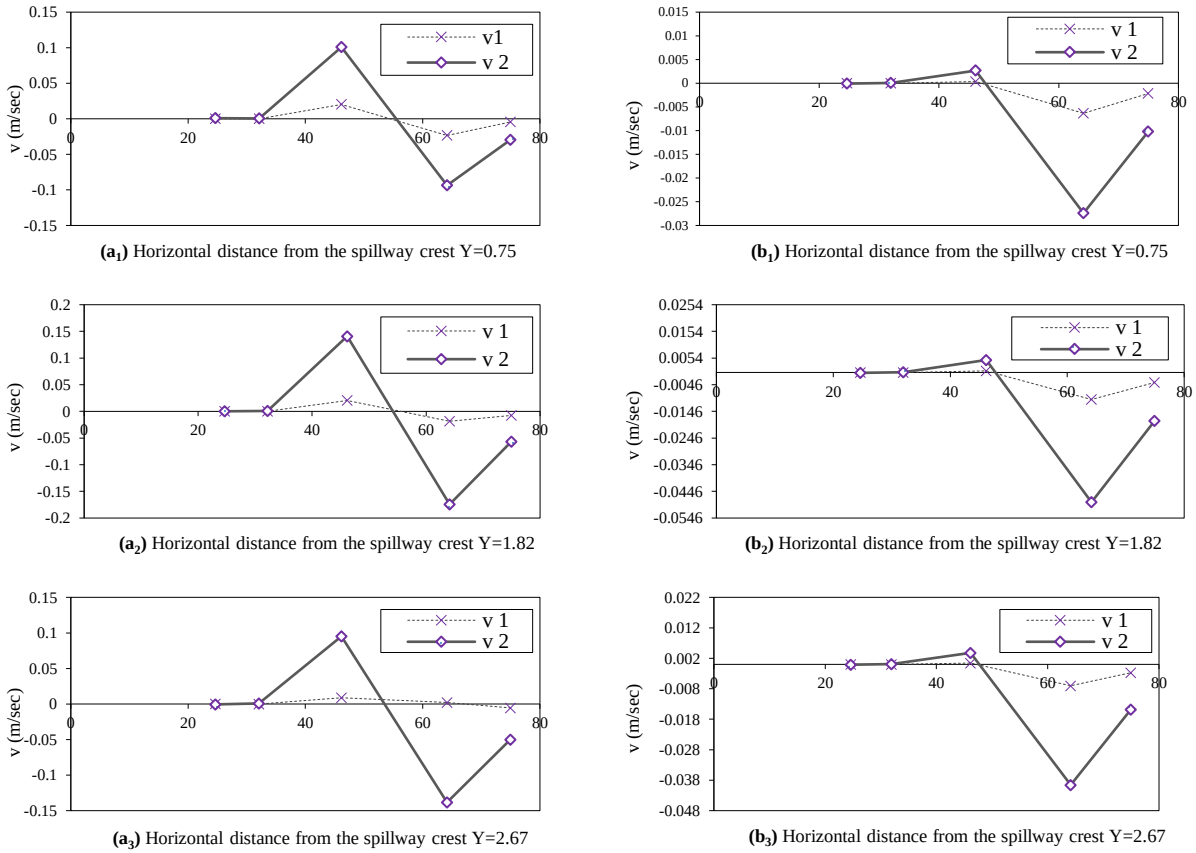


**($a_1$)** Horizontal distance from the spillway crest Y=0.75 **($b_1$)** Horizontal distance from the spillway crest Y=0.75

**($a_2$)** Horizontal distance from the spillway crest Y=1.82 **($b_2$)** Horizontal distance from the spillway crest Y=1.82

**($a_3$)** Horizontal distance from the spillway crest Y=2.67 **($b_3$)** Horizontal distance from the spillway crest Y=2.67

**Fig. 11:** The transverse velocity at various points across the width of the bucket at **($a_{1, 2, \&3}$)** Z=15 and **($b_{1, 2, \&3}$)** Z=19.5 meters from the lowest point of the model. The measurements are taken at **($a_1$)** & **($b_1$)** Y=0.75 m (on the retracted tooth and its corresponding position in the bucket with aligned teeth), **($a_2$)** & **($b_2$)** Y=1.82 m (between the teeth), and **($a_3$)** & **($b_3$)** Y=2.67 m (on the forward tooth in the bucket with zigzag teeth and its corresponding position in the bucket with aligned teeth)

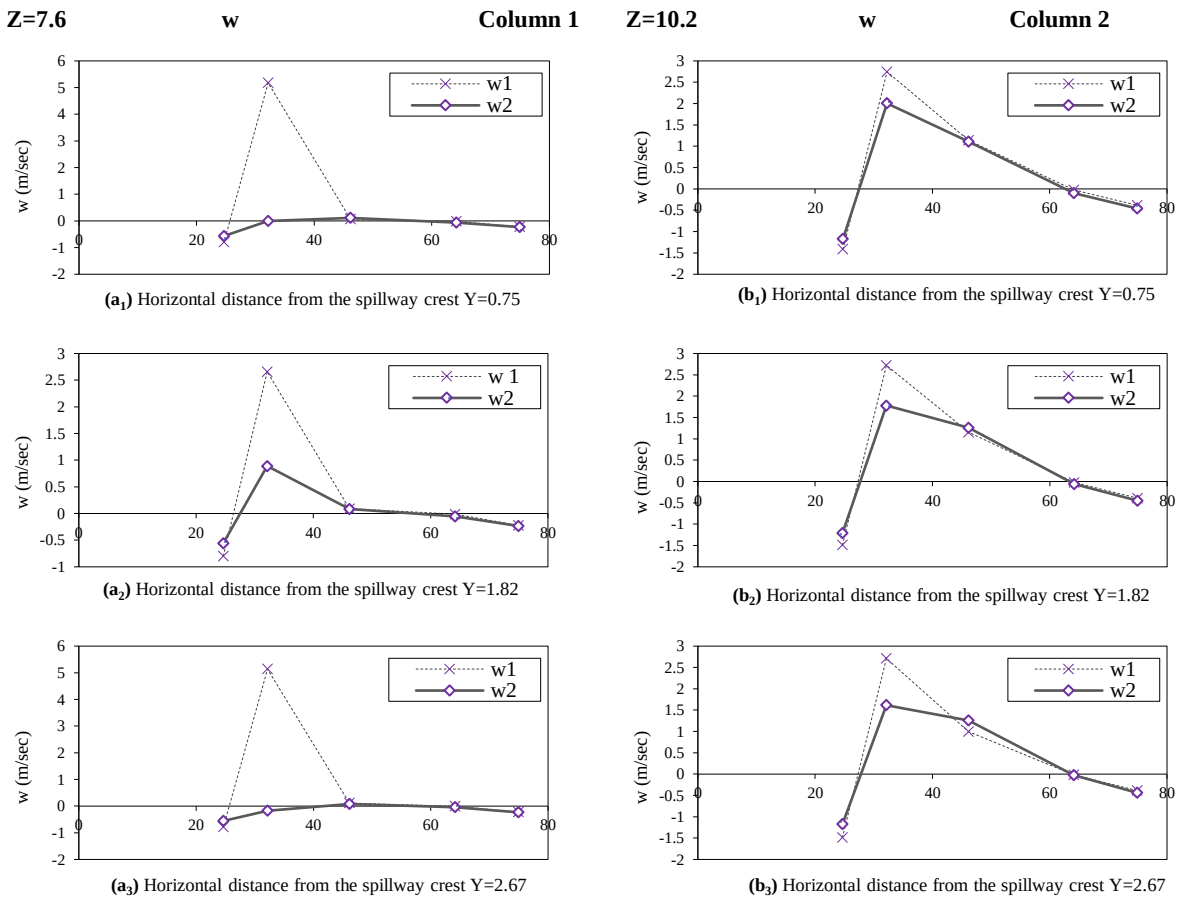


**Fig. 12:** The transverse velocity at various points across the width of the bucket at **($a_{1, 2, \&3}$)** Z=7.6 and **($b_{1, 2, \&3}$)** Z=10.2 meters from the lowest point of the model. The measurements are taken at **($a_1$)** & **($b_1$)** Y=0.75 m (on the retracted tooth and its corresponding position in the bucket with aligned teeth), **($a_2$)** & **($b_2$)** Y=1.82 m (between the teeth), and **($a_3$)** & **($b_3$)** Y=2.67 m (on the forward tooth in the bucket with zigzag teeth and its corresponding position in the bucket with aligned teeth)

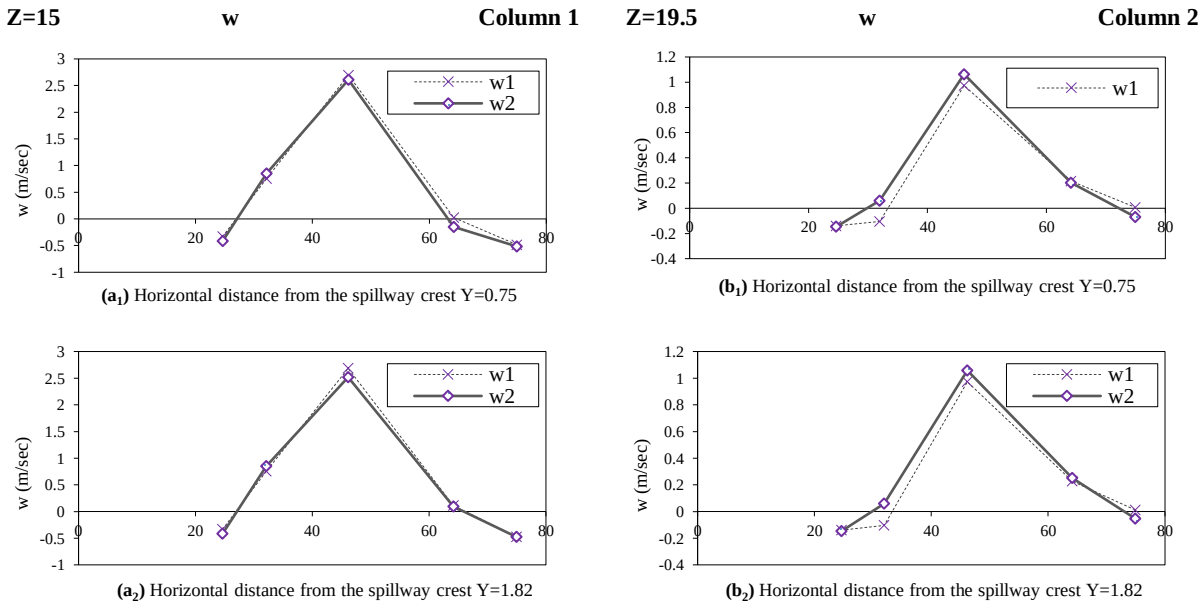

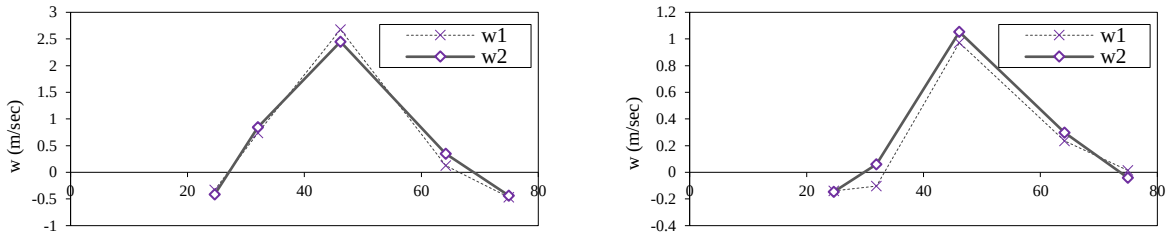


**($a_3$)** Horizontal distance from the spillway crest Y=2.67 **($b_3$)** Horizontal distance from the spillway crest Y=2.67

**Fig. 13:** The transverse velocity at various points across the width of the bucket at **($a_{1, 2, \&3}$)** Z=15 and **($b_{1, 2, \&3}$)** Z=19.5 meters from the lowest point of the model. The measurements are taken at **($a_1$)** & **($b_1$)** Y=0.75 m (on the retracted tooth and its corresponding position in the bucket with aligned teeth), **($a_2$)** & **($b_2$)** Y=1.82 m (between the teeth), and **($a_3$)** & **($b_3$)** Y=2.67 m (on the forward tooth in the bucket with zigzag teeth and its corresponding position in the bucket with aligned teeth)

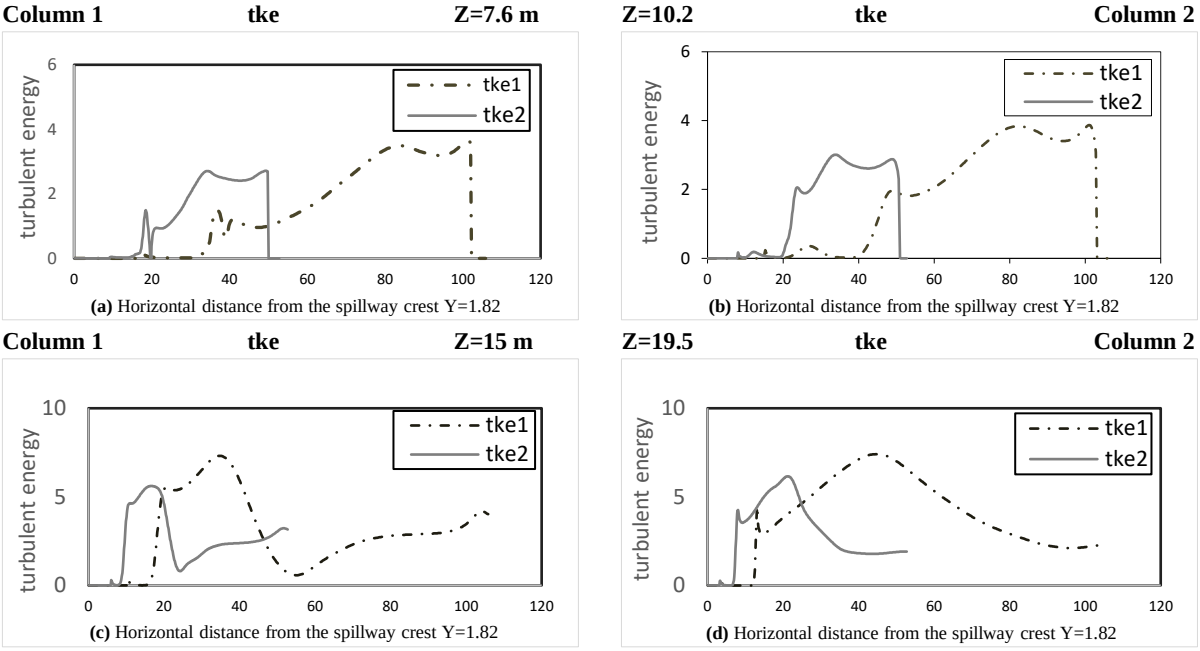


**Fig. 14:** The variations in turbulence energy along the channel, between the teeth, at **(a)** Z=7.6, **(b)** 10.2, **(c)** 15, and **(d)** 19.5 meters from the lowest point of the model. The measurement is taken at Y=1.82 (between the teeth)

## 5. Conclusion

Near the bed (7.6 meters), the flow velocity in the bucket with zigzag teeth (u2) is lower than in the bucket with aligned teeth (u1). This reduction in flow velocity decreases the velocity components that contribute to increased scour. At a height of 10.2 meters, the bucket with zigzag teeth has a lower velocity compared to the bucket with aligned teeth. At higher elevations (15 and 19.5 meters), the velocity in the bucket with zigzag teeth is higher near the bucket and lower downstream compared to the bucket with aligned teeth.

At a height of 7.6 meters, the transverse velocity in the bucket with zigzag teeth is higher. This increase in transverse velocity aids in enhancing flow mixing. At a height of 10.2 meters and above, the transverse velocity in the bucket with zigzag teeth is greater than in the bucket with aligned teeth. This difference in transverse velocity becomes more pronounced as the distance from the bucket increases.

At lower heights (7.6 and 10.2 meters), the vertical velocity in the bucket with zigzag teeth is lower than in the bucket with aligned teeth. This reduction in vertical velocity helps to decrease the flow energy and consequently reduces turbulence and boiling over the

teeth. At higher elevations (15 and 19.5 meters), the vertical velocity in the bucket with zigzag teeth is slightly lower than in the bucket with aligned teeth.
The turbulence kinetic energy at all heights in the bucket with zigzag teeth is lower than in the bucket with aligned teeth. This reduction indicates decreased flow turbulence downstream, resulting in a less turbulent flow that increases stability and reduces energy dissipation.
The alteration of the tooth arrangement from aligned to zigzag has contributed to the improvement of flow characteristics. The reduction in flow velocity near the bed and the decrease in vertical velocity have led to a reduction in the components that generate scouring and have resulted in less turbulence energy in the flow. These changes can lead to reduced scouring and improved flow stability. Overall, these findings indicate that changing the tooth arrangement to a zigzag pattern can help reduce turbulence energy, decrease flow velocity in the vertical direction, and enhance flow stability, which in turn can be effective in the optimal design of hydraulic structures such as roller buckets.

## 6. References


[1] Kahrizi, E., (2024). Application of the Image Processing Method and the Beer-Lambert Law for Assessing Sea Water Intrusion in Rivers. *Numerical Methods in Civil Engineering, 8(4), 37-43.* doi: 10.52547/NMCE.2405.1058

[2] Rahmani Firozjaei, M., Behnamtalab, E. and Salehi Neyshabouri, S.A.A. (2018) Numerical simulation of lateral pipe intake from open channel, Iranian Journal of Soil and Water Research, 50(1), pp. 135-147. doi: 10.22059/ijswr.2018.252260.667851.

[3] Kahrizi, E., Neyshabouri, S.A.A.S., Souri, J., Akbari, H., (2023). Experimental evaluation of two-layer air bubble curtains to prevent seawater intrusion into rivers. Journal of Water and Climate Change14 (2): 543–558. https://doi.org/10.2166/wcc.2023.384

[4] Safravani, F. (1992). Investigation of downstream scour in draft tube cone. M.Sc. Thesis, Hydraulic Structures Engineering, Tarbiat Modares University.

[5] Fathalikhani, M. & Gatmiri, B. (2016). Analysis of coupled thermohydromechanical damage in unsaturated porous media. Amirkabir Journal of Civil Engineering: 48(1), pp. 23-34.

[6] Fathalikhani, M. & Gatmiri, B. (2012). Coupled analysis of damage in multiphase media. Journal of Multiscale Modelling: 4(2), pp. 1250008.

[7] Fathalikhani, M., Graham, J., Kurz, D. & Maghoul, P. (2022). Investigation and modification of a CSSM-based elastic–thermoviscoplastic model for clay. International Journal of Geomechanics: 22(10).

[8] Mason, P.J. & Arumugam, K. (1985). Free jet scour below dams and flip buckets. Journal of Hydraulic Engineering, 111(2), 220-235; 113(9), 1192-1205.

[9] Veronese, A. (1937). Erosions of the riverbed downstream of a discharge. Annals of Public Works, 75(9), 717-176.

[10] Chee, S.P. & Padiyar, P.V. (1969). Erosion at the base of flip buckets. Engineering Journal, Canada, 52(11), 22-24.

[11] Martins, B.F. (1975) Scouring of rocky riverbeds by free-jet spillways, *Journal Name*, 27(4), April, pp.

[12] Strelchuck, D.L., 1969. Scour at the base of spillway buckets. M.S. Thesis, University of Windsor, Ontario.

[13] Azmathullah, H.Md., Deo, M.C., Deolalokar, P.B., 2005. Neural networks for estimation of scour downstream of ski-jump bucket. J. Hyd. Eng., ASCE.

[14] Asadi Sari Zadi, M. (1999). Determining the effect of the simple cylindrical thrower in the lower depths of spillways, M.Sc. Thesis, Civil Engineering Hydraulic Structures, Tarbiat Modares University.

[15] Golzari, F. (2002). The effect of jet dispersion, geometric shape of the cup, and draft depth on the development of washing process in the cup thrower. *Sixth International Seminar on River Engineering, Shahid Chamran University, Ahvaz*.

[16] Amanian, N., 1993. Scouring below a flip bucket spillway. Ph.D. Thesis, Utah State University, Logan, Utah.

[17] Panahi, S., Farsadizadeh, D., Hosseinzadeh Deliri, A., Karimi J. (2011). "Laboratory investigation of scour at the downstream of the cylindrical roller jet thrower

structure under the influence of 45-degree baffle angle. Fifth National Congress of Civil Engineering, Semnan.

[18] Eshtiyagh Hassannejad, F., Farsadizadeh, D., Hosseinzadeh Deliri, A., Abbaspour, M. (2011). Laboratory investigation of sedimentation at the downstream of the baffle energy dissipator with toothed cylindrical rollers. Fifth National Congress of Civil Engineering, Semnan.

[19] Panahi S., Eshtiyagh Hassannejad, F., Farsadizadeh, D., Hosseinzadeh Deliri, A. (2012). "Comparison of scour dimensions at the downstream of the plain and toothed cylindrical roller energy dissipator structures." Ninth International Congress on Civil Engineering, Isfahan University of Technology.

[20] Pétursson, G. (2013) Model investigation of a low Froude number roller bucket at Urriðafoss HEP.

[21] Malcolm H. Karr, Bucket-type Energy dissipator characteristics.

[22] Heidarian, P., Neyshabouri, S.A.A.S., Khoshkonesh, A., Bahmanpouri, F., Nsom, B. and Eidi, A., 2022. Numerical study of flow characteristics and energy dissipation over the slotted roller bucket system. Modeling Earth Systems and Environment, 8(4), pp.5337-5351.

[23] Souri, J., OmidvarMohammadi, H., Neyshabouri, S.A.A.S., Chooplou C.A., Kahrizi, E., Akbari, H., (2024). Numerical simulation of aeration impact on the performance of a-type rectangular and trapezoidal piano key weirs. Model. Earth Syst. Environ. https://doi.org/10.1007/s40808-024-02058-4.

[24] CW (2011) 'CFD-101: The basics of computational fluid dynamics modeling'.

[25] Rahmani Firozjaei, M., Salehi Neyshabouri, S. A. A., Amini Sola, S., & Mohajeri, S. H. (2019). Numerical simulation on the performance improvement of a lateral intake using submerged vanes. Iranian Journal of Science and Technology, Transactions of Civil Engineering, 43, 167-177.

[26] Rahmani Firozjaei, M., Behnamtalab, E., & Salehi Neyshabouri, S. A. A. (2020). Numerical simulation of the lateral pipe intake: flow and sediment field. Water and environment journal, 34(2), 291-304.

[27] Hajebi, Z., Firozjaei, M. R., Naeeni, S. T. O., & Akbari, H. (2024). Hydraulic performance of bottom intake velocity caps using PIV and OpenFOAM methods. Applied Water Science, 14(3), 38.

[28] Naeeni, S. T. O., Rahmani Firozjaei, M., Hajebi, Z., & Akbari, H. (2023). Investigation of the performance of the response surface method to optimize the simulations of hydraulic phenomena. Innovative Infrastructure Solutions, 8(1), 10.

[29] Rahmani Firozjaei, M., Hajebi, Z., Naeeni, S. T. O., & Akbari, H. (2024). Experimental and Numerical Investigation of Bottom Intake Structure for Desalination Plants. Numerical Methods in Civil Engineering, 8(3), 1-9.

[30] Firozjaei, M. R., Naeeni, S. T. O., & Akbari, H. (2023). Evaluation of seawater intake discharge coefficient using laboratory experiments and machine learning techniques. Ships and Offshore Structures, 1-14.

[31] Rahmani Firozjaei, M., & Behnamtalab, E. (2021). Hydraulic Evaluation of Lateral Pipe-intake from Open Channel by Numerical Simulation. Modares Civil Engineering journal, 21(3), 45-60.

[32] Mirzaei, H., Moghim, M.N. and Asadi, M., 2022. Two-dimensional solution of steady free jet and wall jet by strip integration method and its comparison with empirical relationships and numerical modeling. Modeling Earth Systems and Environment, pp.1-11.

[33] Mirzaei, H., Asadi, M., Tootoonchi, H. and Ramezani, A., 2021. Numerical simulation of secondary flow around the open and close groins in channel with movable bed. Modeling Earth Systems and Environment, pp.1-12.

[34] Khoshkonesh, A., Asim, T., Mishra, R., Dehrashid, F.A., Heidarian, P. and Nsom, B., 2022. Study the effect of obstacle arrangements on the dam-break flow. International Journal of Comadem, 25(1), pp.41- 50.

[35] Aghazadeh, K. and Attarnejad, R., 2020. Study of sweetened seawater transportation by temperature difference. Heliyon, 6(3).

[36] Firozjaei, M. R., Hajebi, Z., Naeeni, S. T. O., & Akbari, H. (2024). Discharge performance of a submerged seawater intake in unsteady flows: Combination of physical models and decision tree algorithms. Journal of Water Process Engineering, 60, 105198.

[37] Aghazadeh, K., & Attarnejad, R. (2020). Improved desalination pipeline system utilizing the temperature difference under sub-atmospheric pressure. Water Resources Management, 34(1), 1-19.

[38] Aghazadeh, K. and Attarnejad, R., 2024. Experimental investigation of desalination pipeline system and vapor transportation by temperature difference under sub-atmospheric pressure. Journal of Water Process Engineering, 60, p.105133.